THE TEMPERATURE GRADIENT IN AND AROUND SOLAR MAGNETIC FLUXTUBES

V. A. Sheminova[1], R. J. Rutten[2], L. H. M. Rouppe van der Voort[3]

[1] *Main Astronomical Observatory, NAS of Ukraine*
27 Akademika Zabolotnoho Str., 03680 Kyiv, Ukraine
e-mail: shem@mao.kiev.ua
[2] *Sterrekundig Instituut*
Postbus 80 000, 3508 TA Utrecht, The Netherlands
email: R.J.Rutten@astro.uu.nl
[3] *Institute of Theoretical Astrophysics, Oslo University*
P.O. Box 1029 Blindern, N-0315 Oslo, Norway
email: r.v.d.voort@astro.uio.no

We use spectra covering the outer part of the extended wing of the solar Ca II K line observed at high angular resolution with the Swedish Vacuum Solar Telescope to test standard solar fluxtube models. The wings of the Ca II resonance lines are formed in LTE both with regard to excitation (source function) and to ionization (opacity) and, therefore, sample temperature stratifications in relatively straightforward fashion. We obtain best fits by combining steeper temperature gradients than those in the standard models for both the tube inside and the tube environment. Similarly steep gradients are also determined from a numerical magnetoconvection simulation by the late A. S. Gadun. It is found that the energy balance in the individual magnetic elements appears to be close to radiative equilibrium throughout the photosphere.

INTRODUCTION

Plage and network on the solar surface consist of discrete magnetic elements that have been modelled as magnetostatic fluxtubes since the pioneering work of Spruit [14]. Observationally they are known as filigree (*e.g.*, [3]) and network bright points. They appear bright through the hot-wall radiation which escapes through the relatively empty tube interior, as already proposed by Spruit and ascertained more recently from detailed magnetoconvection simulations.

The extended wings of the Ca II H&K lines in the solar spectrum provide valuable diagnostics of the temperature stratification of the solar photosphere. In this paper we use them to derive such stratification for individual magnetic elements of the type which grouped together constitute active-region plage. So, we follow the classical example of H&K plage modelling by [11], but exploit the subsequent improvement in angular resolution to diagnose individual magnetic elements rather than spatially unresolved plage. Since the advent of high-order adaptive optics at new meter-class solar telescopes promises substantial further advance, our analysis represents a pilot study for Ca II H&K wing spectrometry at yet higher resolution.

We reverted to simple one-dimensional modelling when we found this actually produced results with higher consistency from our high-resolution spectra. Therefore, we make the basic assumption that the fluxtube filling factor approaches unity for the selected bright-point pixels. This is obviously optimistic, but this approach will become increasingly realistic.

OBSERVATIONS

We use a subset of the observations described in [9]. They were obtained with the former Swedish Vacuum Solar Telescope (SVST) on La Palma and consist of simultaneous spectrograms and filtergrams of the leading sunspot of active region NOAA 8704 taken on September 22, 1999 using correlation tracking and frame selection. The spot was located at 20.0° S, 4.0° E, $\mu = 0.88$.

The data reduction included dark-frame subtraction, flat-field division, correction for straylight, and noise filtering as detailed in [9].

Figure 1 displays our data. The strip images at left are a cutout from a filtergram taken with a 12 Å G-band filter centered on $\lambda = 4305$ Å and a cutout of a Ca II K slitjaw filtergram recorded with a 3 Å wide filter

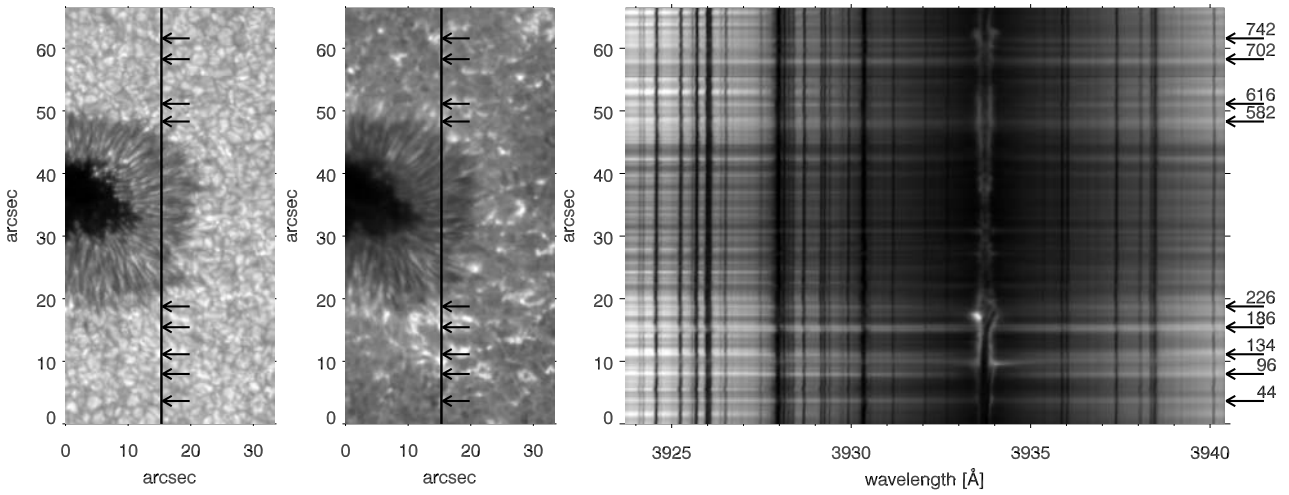

Figure 1. SVST data used in this study, taken on September 22, 1999 of active region AR8704. The two strip images at left are segments of G-band and Ca II K filtergrams, respectively. The superimposed vertical line defines the slit location. The corresponding Ca II K spectrogram is shown at right. The arrows specify the locations along the slit for which we analyse Ca II K wing spectra, identified by their pixel row numbers at right

centered at Ca II K (3933.7 Å). The location of the spectrometer slit is indicated with superimposed vertical lines. The arrows identify the nine bright points selected for this study.

The Ca II K spectrogram at right is a 350 ms exposure with the SVST's Littrow spectrometer. It was taken synchronously with the Ca II K slitjaw filtergram. The slit width of 25 μm corresponds to 0.23 arcsec angular and 30 mÅ spectral resolution. The 9 μm pixel size of the CCD camera corresponds to 11 mÅ spectral and 0.083 arcsec spatial sampling. The telescope diffraction limit was 0.2 arcsec at Ca II K and is nearly reached in this high-quality spectrogram. The selected bright streaks may not be fully resolved but they are relatively well-defined.

METHOD

For each bright point selected in Fig. 1 we derive empirical best-fit models through trial-and-error adjustment of the temperature stratification in a one-dimensional magnetostatic thin-fluxtube model until the computed Ca II K wings match the observed ones. We use the SPANSAT code described by [5] for LTE spectral synthesis of the full overlapping H&K lines including superimposed blends. It computes optical intensity spectra containing any selection of overlapping spectral lines from a given one-dimensional model atmosphere. The spectral line parameters were taken from the VALD database at URL [`http://www.astro.univie.ac.at/~vald`].

A major problem that formerly affected such line-wing synthesis concerned the amount of collisional damping by neutral hydrogen atoms. It was commonly fudged through the application of an arbitrary "damping enhancement factor", but this uncertainty has largely vanished with the quantum-mechanical estimation method of [1] which we apply in our code.

Another classic problem is posed by the "line haze" consisting of the multitude of unresolved weak lines in this part of the spectrum. Unfortunately, this problem remains even in the presence of large spectral line databases. We apply scaling factors to the continuous opacity as computed from the standard sources to mimic its existence.

For each new tube-interior temperature stratification in our trial-and-error fitting, the SPANSAT code is combined with re-computation of the gas and electron pressures assuming vertical hydrostatic equilibrium and including LTE evaluation of the ionization equilibrium for all pertinent elements. The procedure also includes thin-tube horizontal magnetostatic evaluation of the magnetic field stratification. It follows Eqs. (1)–(3) of [2], which fully define isolated thin magnetostatic fluxtubes by the inside and outside temperature stratifications plus the values of the tube radius, field strength, and outside gas pressure at the tube base. The outside model (HSRA-SP-M) and the standard fluxtube model (PLA) from which we take the base values are discussed next.

As outside quiet-Sun model we use a doubly modified version of the HSRA. It was extended as HSRA-SP into deeper layers by [13] taking convective energy transport into account. Our own modification, which we call HSRA-SP-M henceforth, is a Ca II H&K fit to the Brault–Neckel atlas [7]. The corresponding HSRA-SP-M

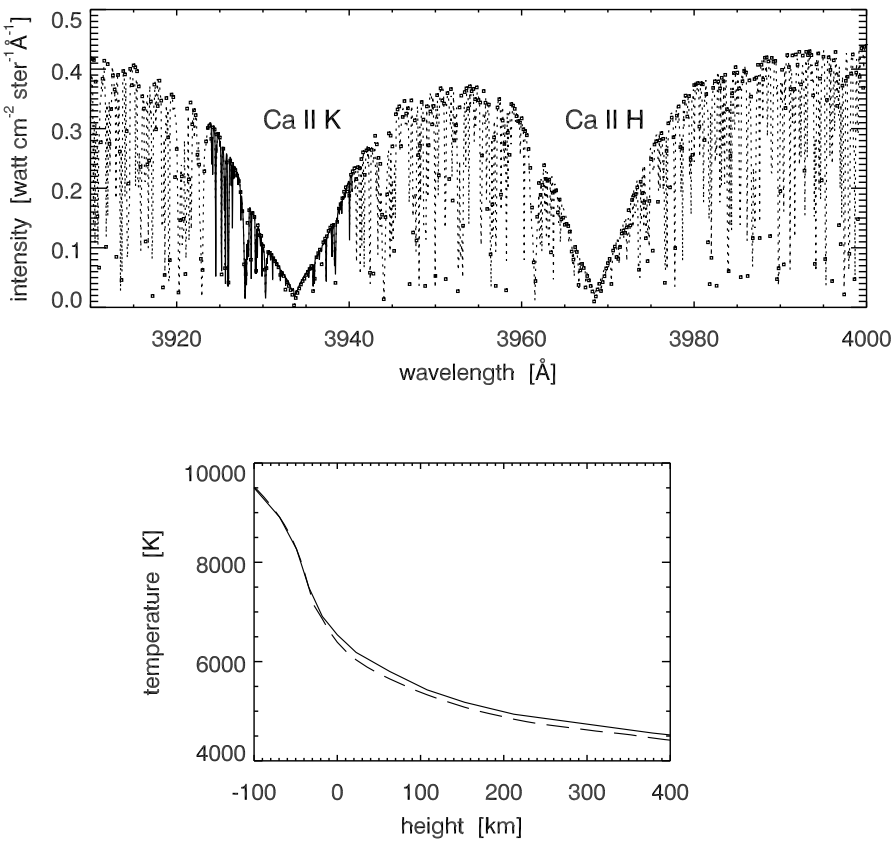

Figure 2. Adaptation of the HSRA-SP standard model. *Up*: solar disc-center intensity spectrum in the Brault–Neckel atlas [7]. The fat solid line marks the segment covered by the spectrogram in Fig. 1. The squares result from spectrum synthesis with HSRA-SP-M which was constructed by fitting the H&K wing windows between blends. *Bottom*: HSRA-SP-M temperature stratification (solid) compared with the HSRA-SP (dashed) models. The height scale has its zero point at $\tau_5 = 1$ for each model

model in the lower panel of Fig. 2 is indeed 100–150 K hotter than the HSRA (or HSRA-SP) in the middle photosphere.

We use the standard fluxtube model PLA for solar plage constructed by [12] as the initial model defining our fluxtube base input parameters. They are a fluxtube diameter of 200 km, field strength of 2500 G, and outside gas pressure of $5 \cdot 10^5$ dyn/cm^2, respectively.

The spectral intensities were calibrated to absolute intensities through the quiet-Sun disc-center fit to the Brault–Neckel atlas obtained with the line-haze corrections and HSRA-SP-M modification described above. Spectral synthesis for $\mu = 0.88$ with these fitting parameters was found to correspond well with the Brault–Neckel atlas. The observed spectrogram brightness scale was then converted into absolute units by matching the average of the quiet-Sun part sampled in the lowest ten pixel rows of our spectrogram (Fig. 1) to this synthetic spectrum.

RESULTS

Figure 3 shows the observed Ca II K wing spectra for the nine selected bright points marked in Fig. 1. The plus symbols in Fig. 3 show the results from our one-dimensional fitting through trial-and-error adjustment of the temperature stratification including recomputation of the hydrostatic densities, ionization equilibrium, continuous and line opacities, and magnetic field stratification. The corresponding best-fit temperature stratifications are shown in Fig. 4, with the HSRA-SP-M and PLA models added for reference. The superimposed symbols mark the model temperatures that equal the observed brightness temperatures at the wavelengths marked by symbols in Fig. 3 for the bright point at pixel row 96 (star symbols) and 582 (plus symbols). They define the height range over which our fitting defines each model most sensitively, and span the variation between the different bright points. The left-hand panels shows the nine best-fit models on the standard height scale, the right-hand panel on the continuum optical depth scale of each model individually. The difference in

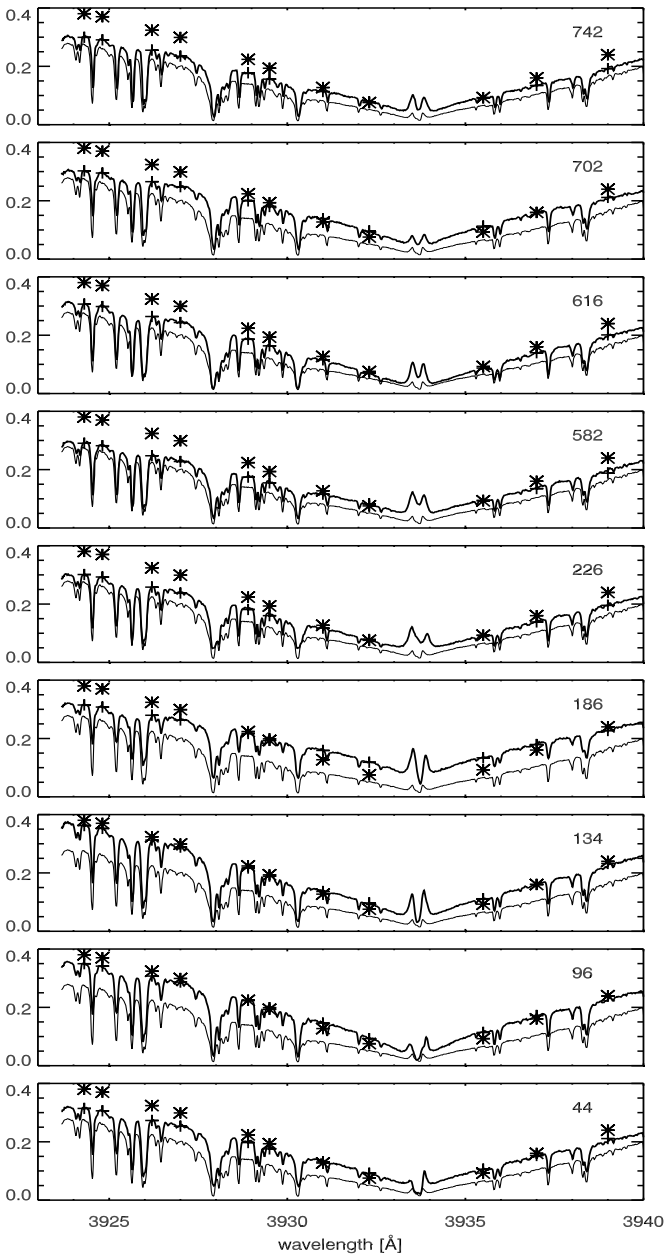

Figure 3. Bright point spectra and model fits. The tracings are absolute intensities derived from the Ca II K spectrogram in units $\mathrm{W\,cm^{-2}\,ster^{-1}\,\AA^{-1}}$. *Thick*: individual bright point spectra. The slit location is indicated by its pixel row number. *Thin*: quiet-Sun average over the lowest 10 pixel rows, repeated in each panel as reference. *Pluses*: absolute intensities from our best-fit model for each bright point. The corresponding temperature stratifications are shown in Fig. 4. *Stars*: absolute intensities computed from the PLA model with spatial "wine-glass" averaging over magnetostatic fluxtubes, the same in each panel

horizontal displacement from the HSRA-SP-M at $T \approx 6500$ K defines the Wilson depression of about 200 km. The nine best-fit models are quite similar. They all show a smooth outward temperature decline cutting through the hump in the PLA model.

COMPARISON WITH NUMERICAL SIMULATION

Figure 5 shows a snapshot from a numerical two-dimensional magnetoconvection simulation by the late A. S. Gadun described in detail in [4] and also employed in [6].

The snapshot is a cutout part of the vertical simulation plane at a location and time where a well-developed, sizeable magnetic element exists which resembles an idealized magnetic fluxtube in its field strength and in being

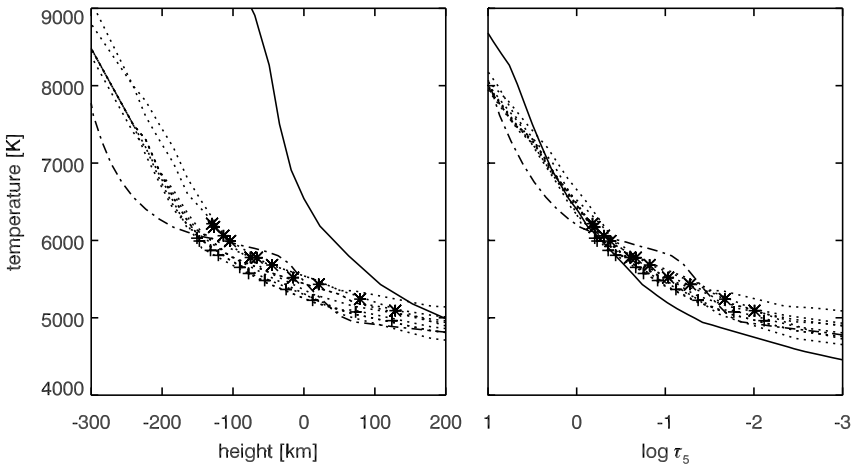

Figure 4. Temperature stratifications of our best-fit bright-point models (9 dotted curves). *Left*: against height. *Right*: against the continuum optical depth at 5000 Å in each model. The marks designate the locations where the fitted model temperatures equal the observed brightness temperatures at the wavelengths marked by symbols in Fig. 3, respectively for spectrogram pixel rows 96 (stars) and 582 (pluses). The HSRA-SP-M (solid) and PLA (dot-dashed) models are added for comparison

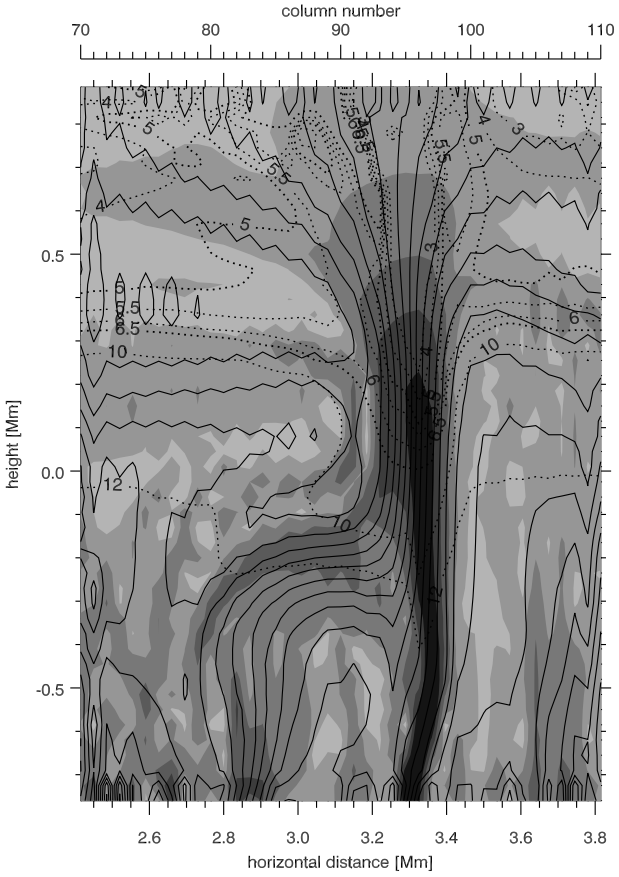

Figure 5. Segment of a snapshot from a numerical magnetoconvection simulation by [4], selected because it contains a strong near-vertical magnetic field concentration reminiscent of an idealized fluxtube. Lighter greyscale shades correspond to field strengths above 2000, 1500, 1000, 500, 200, and 10 G, respectively. Solid curves: magnetic field lines. Dotted curves: isotherms labeled with their temperature value in units of 1000 K

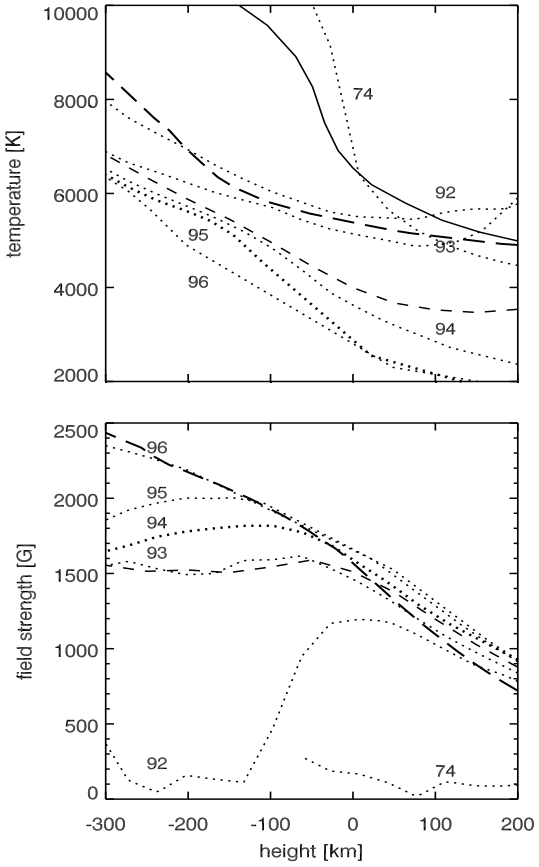

Figure 6. Comparison between bright point models and numerical simulation. Dotted curves: values along snapshot columns as specified by their column numbers in Fig. 5. Thin dashed curves: average over the plotted simulation columns. Thick dashed curves: average of the 9 best-fit bright point models. *First panel*: temperature stratifications. Solid: HSRA-SP-M model. *Second panel*: magnetic field strengths

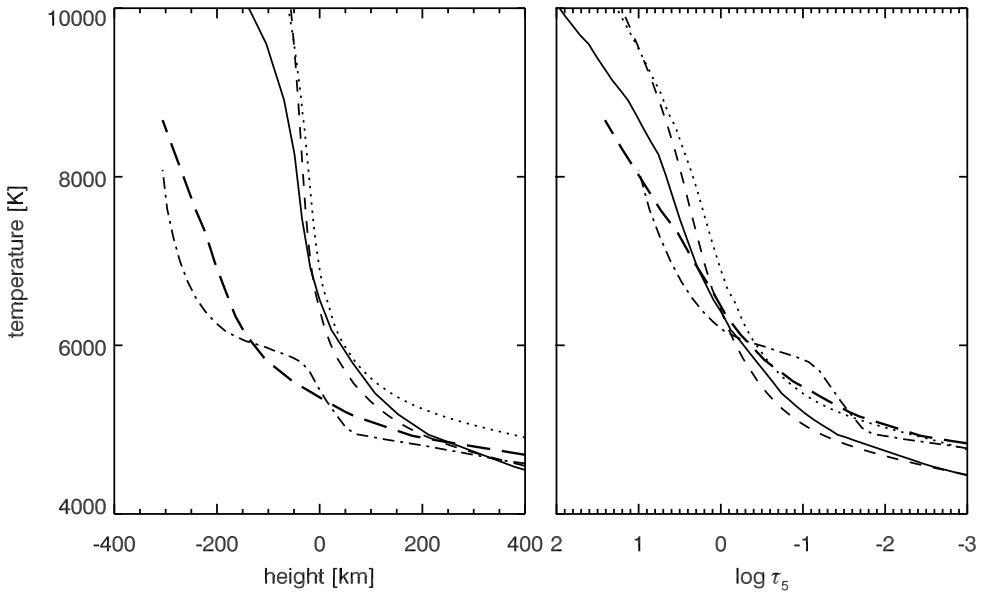

Figure 7. Comparison between bright point models and RE modelling. *Left*: against height. *Right*: against continuum optical depth at 5000 Å in each model. Thick dashed curve: mean of our 9 best-fit bright point models. Thin dashed curve: RE model for $T_{\rm eff} = 5777$ K. Dotted: standard solar RE model for $T_{\rm eff} = 6200$ K. The HSRA-SP-M (solid) and PLA (dot-dashed) models are again added for comparison

fairly straight and vertical. The greyscale coding represents magnetic field strength, the solid curves magnetic field lines, the dotted curves isotherms. The diameter of the magnetic element ranges from 50 km to 200 km depending on contour choice.

The simulated fluxtube is compared to our bright-point measurements in Fig. 6, respectively plotting temperature stratifications (first panel), field stratifications (second panel). In each, the dotted curves are the simulation stratifications along the adjacent columns 92–96, marked by their column number as specified along the top of Fig. 5. The thin dashed curve in each panel is the spatial average over these magnetic-element columns.

The dotted curves for column 74 sample a location without much magnetic field, as representative of the outside quiet Sun. The HSRA-SP-M is added for comparison in the first panel. Of course, the latter represents a spatial average over granulation whereas column 74 is just one sample through a granule interior. Indeed, it shows an upflow and is hotter than HSRA-SP-M below the surface while cooler higher up.

The thick dashed curve in each panel is the corresponding average over the 9 best-fit bright point models. The overall correspondence between the best-fit models and the simulation stratifications is quite good with respect to temperature and field strength. Both the values and the gradients concur rather well. If the simulation is taken to be realistic, the agreement implies that our spectra are representative of comparable magnetic elements in the real Sun without too much resolution loss. Obviously, the temperature gradients across the simulated fluxtube produce appreciable variation between adjacent columns which are only 35 km (less than 0.1 arcsec) apart and thus remains unresolved at our resolution (even though the Ca II K wings should render it faithfully at some modulation response thanks to LTE response).

COMPARISON WITH RE MODELLING

In Fig. 7 we compare our best-fit bright point models with standard plane-parallel radiative-equilibrium (RE) modelling. The thick dashed curve is the mean of our best-fit models. The solid and dot-dashed curves are again the HSRA-SP-M and PLA models, for comparison. Two RE models are added, for $T_{\rm eff} = 5777$ K (thin dashed) and $T_{\rm eff} = 6200$ K (dotted), respectively, with solar values for the other parameters ($\log g = 4.44$, solar abundances). They were kindly computed by Ya. V. Pavlenko using his modification [8] of the ATLAS12 code.

Comparison shows that HSRA-SP-M is close to RE above $\log \tau_5 \approx 0$, confirming the well-known property of the solar photosphere to by-and-large obey radiative equilibrium, as established originally by [10]. The hotter RE model, of which the effective temperature is selected to reproduce that of the bright-point average, is nearly the same above $\log \tau_5 \approx -0.4$. This suggests that also fluxtube photospheres obey radiative equilibrium, *i.e.*, that the non-radiative heating which causes the K_2 emission peaks observed in Fig. 3 sets in only at

larger height. Below the surface both the outside HSRA-SP-M and the mean bright-point interior models have shallower temperature gradients than the RE models.

CONCLUSION

The extended wings of Ca II H&K provide relatively straightforward diagnostics of the temperature stratification in the solar photosphere. We have used them to diagnose nine individual bright points describing individual magnetic elements in a plage area near a sunspot by trial-and-error fitting of high-resolution Ca II K spectrograms. Our main results are that the averaged behaviour corresponds well to a strong-field fluxtube-like magnetic concentration in a magnetoconvection simulation (Fig. 6) and that the energy balance in these elements appears to be close to radiative equilibrium throughout the photosphere (Fig. 7).

Acknowledgements. We are grateful to the observing staff of the SVST for much assistance, to Sami Solanki for sharing his fluxtube codes, to Yakiv Pavlenko for computing the RE models, to Luis Bellot Rubio for advice on magnetostatic modelling, and to Daniel Roy for earlier insights from similar modelling of the outer Ca II H wings. The SVST was part of the Spanish Observatorio del Roque de los Muchachos of the Instituto de Astrofísica de Canarias and operated by the Royal Swedish Academy of Sciences. Our Utrecht–Oslo collaboration is part of the European Solar Magnetism Network supported by the European Commission under contract HPRN-CT-2002-00313, which also funds L. H. M. Rouppe van der Voort. Our Kyiv–Utrecht collaboration is supported by INTAS under contract 00-00084. V. A. Sheminova acknowledges hospitality at Utrecht. R. J. Rutten acknowledges travel support from the Leids Kerkhoven–Bosscha Fonds and hospitality in Kyiv.

[1] *Barklem P. S., O'Mara B. J.* The broadening of strong lines of Ca^+, Mg^+ and Ba^+ by collisions with neutral hydrogen atoms // Astron. and Astrophys.–2002.–**389**, N 3.–P. 863–871.

[2] *Bellot Rubio L. R., Ruiz Cobo B., Collados M.* Response functions for the inversion of data from unresolved solar magnetic elements // Astron. and Astrophys.–1996.–**306**, N 2.–P. 960–972.

[3] *Dunn R. B., Zirker J. B.* The Solar Filigree // Solar. Phys.–1973.–**33**, N 2.–P. 281–304.

[4] *Gadun A. S.* Two-dimensional nonstationary magnetogranulation // Kinematics and Physics of Celestial Bodies.–2000.–**16**, N 2.–P. 99–120.

[5] *Gadun A. S., Sheminova V. A.* SPANSAT: Program for LTE-calculation Absorption Line Profiles in Stellar Atmospheres.–Kiev: Inst. Theor. Phys., 1988.–37 p.–(Preprint N 87P).

[6] *Gadun A. S., Solanki S. K., Sheminova V. A., Ploner S. R. O.* A formation mechanism of magnetic elements in regions of mixed polarity // Solar. Phys.–2001.–**203**, N 1.–P. 1–7.

[7] *Neckel H.* Announcement "Spectal atlas of solar absolute disk-averaged and disk-center intensity from 3 290 to 12 510 Å" (Brault and Neckel, 1987) (Now available from the Hamburg Observatory anonymous ftp-site) // Solar. Phys.–1999.–**184**, N 2.–P. 421–422.

[8] *Pavlenko Ya. V.* Model Atmospheres of Red Giants // Astron. Rep.–2003.–**47**, N 1.–P. 59–67.

[9] *Rouppe van der Voort L. H. M.* Penumbral structure and kinematics from high-spatial-resolution observations of Ca II K // Astron. and Astrophys.–2002.–**389**, N 2.–P. 1020–1038.

[10] *Schwarzschild K.* // Nachrichten Koniglichen Gesellschaft Wissensch.–Gottingen: Math.-Phys. Klasse, 1906.–**195**.–P. 41.

[11] *Shine R. A., Linsky J. L.* A Facular model based on the wings of the Ca II lines // Solar. Phys.–1974.–**37**, N 1.–P. 145–150.

[12] *Solanki S. K., Brigljevic V.* Continuum brightness of solar magnetic elements // Astron. and Astrophys.–1992.–**262**, N 2.–P. L29–L32.

[13] *Spruit H. C.* A model of the solar convection zone // Solar. Phys.–1974.–**34**, N 2.–P. 277–290.

[14] *Spruit H. C.* Pressure equilibrium and energy balance of small photospheric fluxtubes // Solar. Phys.–1976.–**50**, N 2.–P. 269–295.